

IEEE 2009 Custom Intergrated Circuits Conference (CICC)  
**Challenges in the Design of Cognitive Radios<sup>1</sup>**

Behzad Razavi  
Electrical Engineering Department  
University of California, Los Angeles

### Abstract

**Cognitive radios are expected to perform spectrum sensing and communication in the frequency range of tens of megahertz to about 10 GHz. As such, they pose tough architecture and circuit design problems. This paper deals with issues such as broadband, low-noise amplification, multi-decade carrier frequency synthesis, and spectrum sensing. The paper also describes the effect of nonlinearity and local oscillator harmonics, demonstrating that cognitive radios entail more difficult challenges than do software-defined radios. Multi-decade synthesis techniques and RF-assisted sensing methods are also presented.**

### I. INTRODUCTION

The congestion in pre-allocated parts of the frequency spectrum continues to rise as more users access wireless networks. Cognitive radios (CRs) offer an approach to alleviating the congestion: they continually sense the spectrum and detect and utilize unoccupied channels [1, 2]. While present efforts in CR design have focused on the TV bands below 1 GHz [3], it is expected that CRs will eventually operate from tens of megahertz to about 10 GHz (denoted herein by  $BW_{CR}$ ).

This paper describes architecture and circuit design issues facing cognitive radio realizations. The challenges include broadband amplification, mixing spurs due to local oscillator (LO) harmonics, multi-decade LO synthesis, and spectrum sensing with the aid of RF and analog functions in a receiver. A number of synthesis and sensing techniques are also introduced.

Section II makes a brief comparison between CRs and software-defined radios (SDRs). Section III is concerned with the design of the signal path and Section IV with the design of the LO path. Section V presents spectrum sensing methods and proposes approaches to speeding up this task.

### II. COGNITIVE RADIOS VERSUS SOFTWARE-DEFINED RADIOS

A wireless transceiver operating across two to three decades of frequencies may be perceived as a “supersized” software-defined radio. However, several attributes of CR systems make them more challenging than SDRs.

1. Unlike SDRs, which target certain standards and their allocated bands, cognitive radios must operate at *any* frequency in the entire range. This requirement constrains the tolerable ripple in the signal path frequency response and, more importantly, demands synthesizers that provide a carrier frequency from tens of megahertz to about 10 GHz in small steps (e.g., 30 kHz).
2. While SDRs are typically designed with a priori knowledge of the interfering frequency bands (e.g., a radio operating in the 900-MHz GSM band must withstand blockers in the 2-GHz WCDMA band), cognitive radios must tolerate interferers at any frequency in  $BW_{CR}$ . Consequently, the mixing spurs and performance parameters such as the third and second intercept points ( $IP_3$  and  $IP_2$ , respectively) must satisfy more stringent bounds.
3. Unlike SDRs, CRs must sense and detect unoccupied channels, a difficult and slow task that places great demands on the RF and analog functions of the system (Section V).

### III. SIGNAL PATH DESIGN

The multi-decade bandwidth required of future cognitive radios can be viewed as a concatenation of the traditional TV tuner frequency range (tens of megahertz to about 900 MHz), the cellular and wireless LAN frequency range (900 MHz to a few gigahertz), and the ultra-wideband (UWB) frequency range (3 GHz to 10 GHz). In addition to the very large “fractional” bandwidth, CR systems must also tolerate various interferers appearing in these bands.

#### A. Low-Noise Amplifiers

A CR receiver (RX) must provide a relatively flat gain and a reasonable input return loss across  $BW_{CR}$ , making it difficult to employ traditional RF circuit techniques. For example, switched-band circuits or staggered tuning (cascade of stages with staggered resonance frequencies) prove impractical for such a large bandwidth. Recent work on UWB systems has targeted a similar problem, e.g., [4], but the solutions are still inadequate for CRs.

The design of broadband low-noise amplifiers (LNAs) is governed by trade-offs between input matching, noise figure, gain, bandwidth, and voltage headroom. The choice of the topology begins with the input matching requirement. The input matching of the LNA can assume one of several forms:

<sup>1</sup>This work was supported by Realtek Semiconductor and DARPA.

(1) a common-source (CS) stage with inductive degeneration, (2) a common-gate (CG) stage, (3) a gain stage with resistive feedback, (4) a combination of CS and CG stages. The first approach does not lend itself to broadband operation and is hence dismissed. Figure 1(a) shows an example of the second

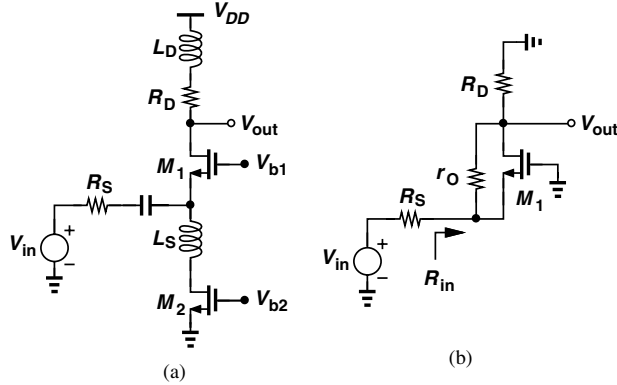


Fig. 1. (a) Common-gate stage, (b) equivalent circuit.

approach, where  $L_S$  resonates with the capacitances in the input network, improving the return loss, and  $L_D$  with the capacitance at the output, extending the bandwidth.

In addition to a relatively high noise figure ( $\geq 1 + \gamma$ , where  $\gamma$  denotes the excess noise coefficient of  $M_1$ ), the circuit of Fig. 1(a) suffers from other drawbacks as well. First, unlike narrowband designs, in which  $M_2$  and  $R_D$  can be replaced with a short circuit, this broadband topology faces severe headroom-gain-noise trade-offs. If body effect and channel-length modulation are neglected and the input is matched, the mid-band noise figure of the circuit is given by

$$NF = 1 + \gamma + \gamma g_{m2} R_S + \frac{4R_S}{R_D}. \quad (1)$$

This expression dictates that  $g_{m2} \ll g_{m1} (= R_S^{-1})$  and  $R_D \gg R_S$ . That is, both the overdrive voltage of  $M_2$  and the dc drop across  $R_D$  must remain much greater than the overdrive of  $M_1$ , requiring a high supply voltage.

The second drawback of the circuit stems from channel-length modulation in deep-submicron devices. From the simplified mid-band equivalent circuit shown in Fig. 1(b), we have

$$R_{in} = \frac{R_1 + r_O}{1 + (g_m + g_{mb})r_O}, \quad (2)$$

and

$$\frac{V_{out}}{V_{in}} = \frac{(g_m + g_{mb})r_O + 1}{r_O + (g_m + g_{mb})r_O R_S + R_S + R_1} R_1. \quad (3)$$

Setting  $R_{in}$  equal to  $R_S$  and using the result in (3), we obtain [5]

$$\frac{V_{out}}{V_{in}} = \frac{(g_m + g_{mb})r_O + 1}{2(1 + r_O/R_1)}. \quad (4)$$

Since  $r_O$  is on the order of  $R_D$ , the voltage gain of this stage is limited to roughly one-fourth of the transistor's intrinsic gain, hardly exceeding 3 (10 dB). Thus, the noise of the following stage may contribute significantly to the receiver noise figure.

Let us now consider the CG/CS combination shown in Fig. 2. Here, the CS stage provides additional voltage gain and,

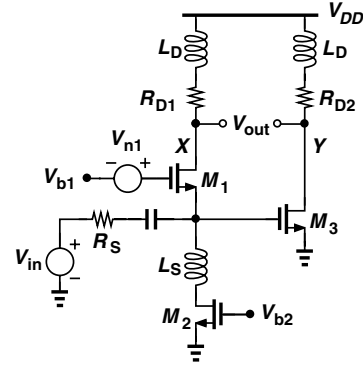


Fig. 2. CG/CS stage.

more importantly, forms a differential output along with the CG stage if  $g_{m1} \approx g_{m3}$  and  $R_{D1} = R_{D2}$ . An interesting property of this circuit is that the noise of  $M_1$ ,  $V_{n1}$ , is canceled [6]. This can be seen by neglecting body effect and channel-length modulation and writing

$$\frac{V_X}{V_{n1}} = -\frac{R_{D1}}{g_{m1}^{-1} + R_S} \quad (5)$$

and

$$\frac{V_Y}{V_{n2}} = -\frac{R_S}{g_{m1}^{-1} + R_S} g_{m3} R_{D2}. \quad (6)$$

Thus, with  $R_{D1} = R_{D2}$  and  $g_{m3} R_S = 1$ ,  $V_{n1}$  emerges only as a common-mode component at the output. However, the overall noise figure is only slightly lower than that of the simple CG stage:

$$NF = 1 + \gamma + \gamma g_{m2} R_S + \frac{2R_S}{R_D}. \quad (7)$$

The topology of Fig. 2 still suffers from the drawbacks of the CG LNA shown in Fig. 1(a), facing serious headroom issues. Furthermore, the additional capacitance contributed by  $M_3$  to the input degrades the  $S_{11}$ .

The concept of noise cancellation can be generalized as follows [6]. If a circuit contains two nodes at which the input signal appears with *opposite* polarities and the noise of a device with the *same* polarity, then the latter can be canceled. As illustrated in Fig. 3(a) [6], proper weighting and summation of the voltages at nodes  $X$  and  $Y$  retains the signal while removing the effect of  $V_{n1}$ . With  $V_{in}$  set to zero, we have

$$V_X = -\frac{g_{m1}(R_S + R_F)}{1 + g_{m1}R_S} V_{n1} \quad (8)$$

$$V_Y = -\frac{g_{m1}R_S}{1 + g_{m1}R_S} V_{n1}. \quad (9)$$

On the other hand, with  $V_{n1}$  set to zero,

$$V_X = \frac{1}{1 + g_{m1}R_S} V_{in} \quad (10)$$

$$V_Y = \frac{1 - g_{m1}R_F}{1 + g_{m1}R_S} V_{in}. \quad (11)$$

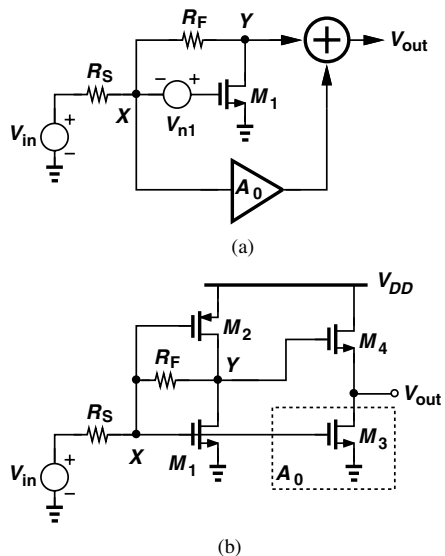


Fig. 3. (a) Noise-canceling LNA, (b) implementation of (a).

Thus, if  $A_0$  is chosen equal to  $-(1 + R_F/R_S)$ , then  $V_{out}$  is free from the noise of  $M_1$  and equal to

$$V_{out} = -\frac{R_F}{R_S}V_{in}. \quad (12)$$

Of course, the noise of the auxiliary amplifier,  $A_0$ , must be sufficiently small.

Figure 3(b) depicts an implementation of the idea [6]. Here,  $M_3$  serves as the auxiliary amplifier and  $M_4$  as the summer. Note that the noise of  $M_2$  is also canceled; if operating as a *constant* current source,  $M_2$  would contribute substantial noise due to the limited headroom.

The cancellation technique described above also suppresses nonlinear components produced by the input device [6] even though they are correlated with the input signal. The linearity of the LNA is thus limited by that of the auxiliary amplifier.

The principal drawback of the noise-cancellation technique shown in Fig. 3(a) relates to the noise of the *auxiliary* amplifier. If modeled as an input-referred voltage of  $\overline{V_{n,aux}^2}$ , this noise is amplified by a factor of  $(1 + R_F/R_S)^2$  as it appears at the output. Dividing this result by  $(R_F/R_S)^2$ , we obtain  $(1 + R_S/R_F)^2 \overline{V_{n,aux}^2}$ , i.e.,  $\overline{V_{n,aux}^2}$  is referred to the main input by a factor of at least unity (for  $R_S \ll R_F$ ). To minimize this contribution, the auxiliary amplifier must incorporate large transistors, thereby degrading the  $S_{11}$  (and the noise and distortion cancellation) at high frequencies.

### B. Nonlinearity and LO Harmonics

In addition to third-order intermodulation, several other phenomena in cognitive radios corrupt the signal path in the presence of large interferers. Specifically, cognitive receivers must satisfy more stringent  $IP_2$  requirements than must SDRs. To understand this point, let us consider the effect of even-order distortion in the signal path in direct-conversion narrowband and software-defined radios. As illustrated in Fig. 4(a), two interferers at  $f_1$  and  $f_2$  generate a beat at  $f_2 - f_1$  as they

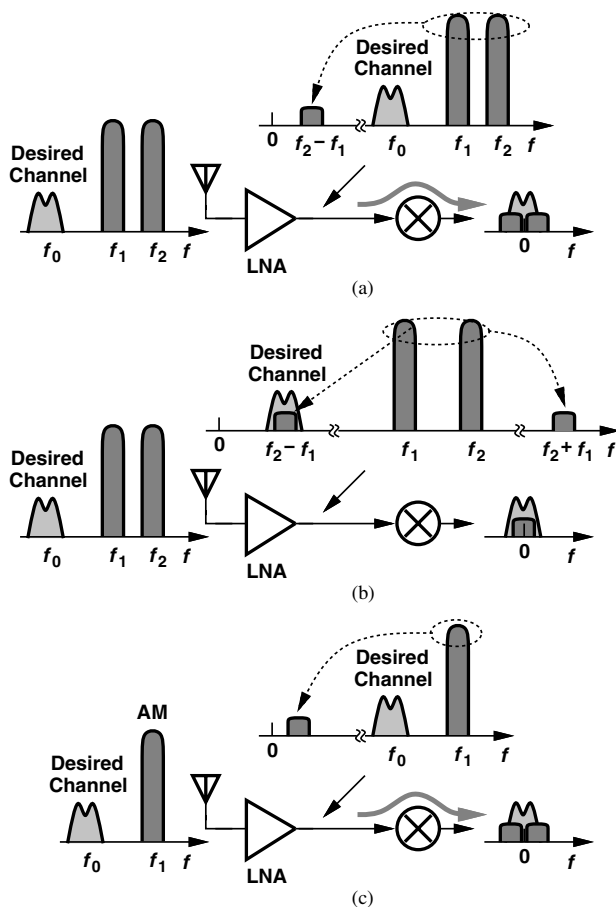


Fig. 4. (a) Even-order distortion in narrowband receivers, (b) even-order distortion in broadband receivers, (c) effect of amplitude-modulated interferers.

experience even-order distortion in the LNA and the input stage of the mixer. Owing to random asymmetries within the mixer, a fraction of this beat leaks to the baseband without frequency translation, corrupting the downconverted signal. In this scenario, only the mixer limits the performance because ac coupling of the LNA output can remove its low-frequency beats. Indeed, the  $IP_2$  of most receivers is measured according to this scenario, and significant effort has been expended on improving the  $IP_2$  of mixers [7, 8].

The problem of even-order nonlinearity assumes new dimensions in cognitive radios. As shown in Fig. 4(b), the LNA itself produces components at  $f_2 + f_1$  and  $f_2 - f_1$ , both of which may lie within  $BW_{CR}$ . That is, the LNA becomes the bottleneck. Differential topologies alleviate this issue considerably, but it is extremely difficult to design low-loss baluns having a bandwidth of two to three decades.

Another effect arising from even-order distortion is the beat resulting from the demodulation of AM interferers [Fig. 4(c)]. Since the envelope component of most modulation schemes used in wireless standards exhibits a bandwidth less than a few tens of megahertz, this beat falls below  $BW_{CR}$  and can be filtered by ac coupling of the LNA output. However, the input stage of the mixer also suffers from this effect, dictating

adequate  $IP_2$  in the mixer.

It is useful to determine bounds on the necessary values of  $IP_2$  and  $IP_3$  in cognitive radios. A plausible approach is to assume the intermodulation components resulting from second- and third-order nonlinearity have equal magnitudes for a certain input level in a two-tone test [Fig. 5(a)]. Denoting

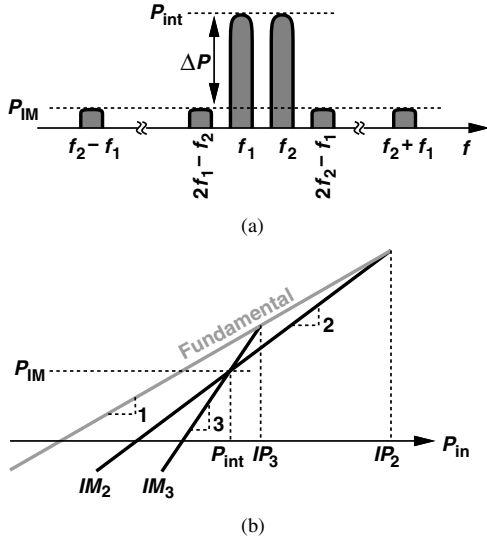


Fig. 5. (a) Input power level producing equal  $IM_2$  and  $IM_3$  products, (b) illustration of  $IM_2$ -limited and  $IM_3$ -limited regions.

this level by  $P_{int}$  and expressing the quantities in dB and dBm, we have  $\Delta P = P_{int} - P_{IM}$  and

$$\Delta P + P_{int} = IP_2 \quad (13)$$

$$\frac{\Delta P}{2} + P_{int} = IP_3. \quad (14)$$

Thus,

$$2P_{int} - P_{IM} = IP_2 \quad (15)$$

$$3P_{int} - P_{IM} = 2IP_3. \quad (16)$$

That is,

$$P_{int} = 2IP_3 - IP_2. \quad (17)$$

For example, if  $IP_3 = -5$  dBm and  $IP_2 = +30$  dBm, then  $P_{int} = -40$  dBm; i.e., the system tends to be  $IM_2$ -limited for interferers below this level and  $IM_3$ -limited for interferers above this level [Fig. 5(b)].

As with SDRs, the downconversion and upconversion mixing in cognitive radios must deal with the LO harmonics. As shown in Fig. 6(a) for the receive path, the harmonics of the LO can mix with interferers, corrupting the downconverted desired signal. Unlike SDRs, however, the decades-wide bandwidth of cognitive radios makes high-order LO harmonics still critical. For example, an SDR operating in the range of 900 MHz to 5 GHz need deal with harmonics up to the fifth or sixth order whereas a CR accommodating the range of 100 MHz to 10 GHz must handle harmonics up to the 100-th order!

Recent work on SDRs has focused on harmonic-rejection mixers [9, 10] derived from the original concept in [11]. Illustrated in Fig. 6(b), the idea is to mix the RF signal with

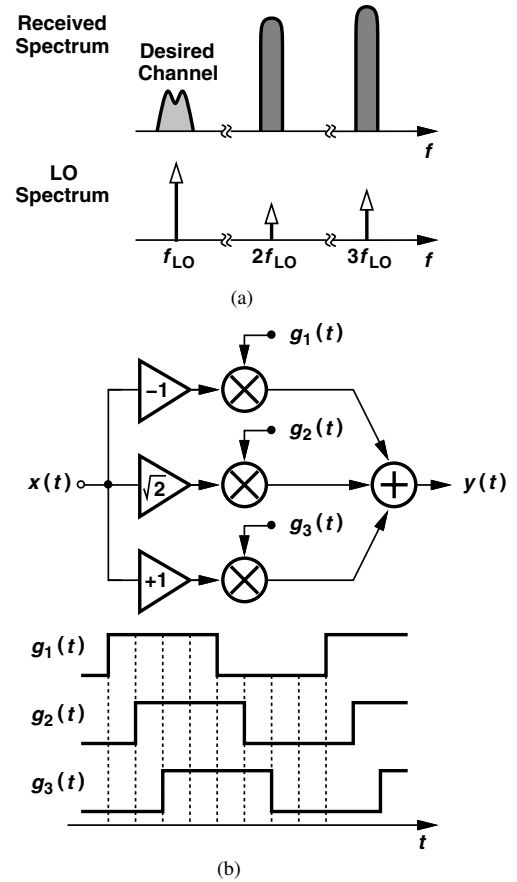


Fig. 6. (a) Effect of LO harmonics in a broadband receiver, (b) harmonic-rejection mixing.

multiple phases of the LO,  $g_1(t)$ - $g_3(t)$ , and sum the results with proper weighting so as to cancel the effect of the third and fifth harmonics. It can be shown that if  $x(t)g_2(t)$  is scaled by a factor of  $\sqrt{2}$  with respect to  $x(t)g_1(t)$  and  $x(t)g_3(t)$ , then these harmonics are removed [11]. With typical mismatches, the effect of the harmonics is reduced by 30 to 40 dB.

If applied to cognitive radios, harmonic-rejection mixing faces several critical issues. First, even for third and fifth harmonics, it requires the generation and distribution of eight LO phases, a difficult task as the LO frequency reaches a few gigahertz (the maximum LO frequency whose harmonics prove troublesome). Second, harmonic mixing becomes very complex if harmonics of seventh and higher orders must be rejected. Third, this technique does not remove *even* LO harmonics that result from random asymmetries in the mixers or LO waveforms. Consider, for example, the single-balanced mixer shown in Fig. 7(a), with  $V_{OS}$  modeling the  $V_{GS}$  mismatch between  $M_2$  and  $M_3$ . As illustrated in Fig. 7(b), the resulting vertical shift in the LO waveform equivalently distorts the duty cycle of the switching of  $M_2$  and  $M_3$ . It can be shown that the second LO harmonic arising from this effect has a peak amplitude of

$$\frac{V_{2LO}}{V_{LO}} \approx \frac{4}{\pi} \frac{V_{OS}}{V_{LO}}, \quad (18)$$

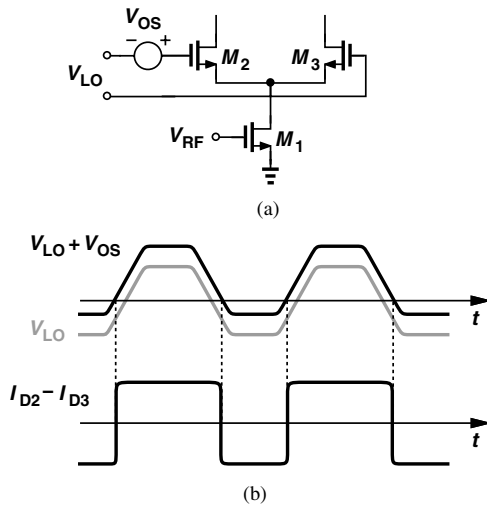


Fig. 7. (a) Single-balanced mixer with offset in LO path, (b) effect of offset on duty cycle of current switching.

where  $V_{LO}$  denotes the peak amplitude of the differential LO waveform. If  $V_{OS} = 10$  mV and  $V_{LO} = 400$  mV, then the second harmonic is only 30 dB below the fundamental.

By virtue of their spectrum sensing capability, cognitive radios may cope with the LO harmonics at the system level. Suppose, as shown in Fig. 8, a desired channel at  $f_1$  must be

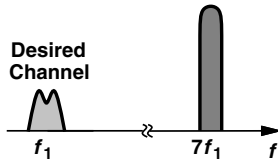


Fig. 8. Desired signal along with an interferer that cannot be removed by harmonic-rejection mixing.

sensed to determine availability. Since  $f_1$  is known, the CR may first sense the channel at  $7f_1$  and determine whether it is occupied by an interferer. If so, the receiver may simply discard the channel at  $f_1$  and seek another for communication. Note that the sensing of the interferer takes little time because only large levels are problematic. In essence, CRs can afford such generosity because they utilize a wide frequency range.

#### IV. LO PATH DESIGN

As mentioned in Section II, the generation of the LO frequencies becomes more challenging in CRs than SDRs. The tuning range of  $LC$  oscillators hardly exceeds  $\pm 15\%$  if a reasonable phase noise must be maintained, making decade-wide coverage difficult. Of course, frequency dividers can be used to generate lower decades.

Carrier synthesis for cognitive radios must follow three principles:

1. Each frequency component must be produced in quadrature form without the use of lossy, power-hungry polyphase filters.
2. Due to its large spurious content, single-sideband (SSB) mixing must be avoided.

3. Except for a particular approach described below, if a frequency is divided by an odd number, it must then be divided by 4 so as to generate quadrature phases.

Based on these principles, one decade of carrier frequencies can be produced as shown in Fig. 9. Employing a single

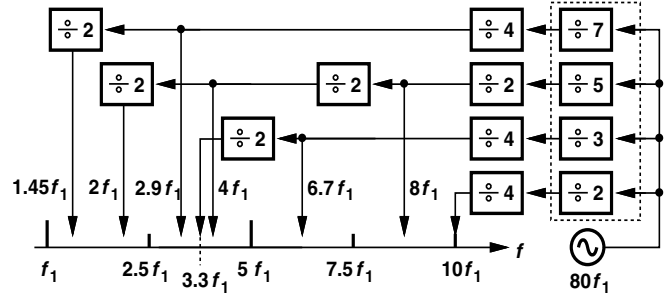


Fig. 9. Generation of one decade of frequencies using a single LO.

oscillator running at  $80f_1$  and six divider chains, the circuit synthesizes quadrature carrier phases at  $10f_1$ ,  $8f_1$ ,  $6.7f_1$ ,  $4f_1$ ,  $3.3f_1$ ,  $2.9f_1$ ,  $2f_1$ , and  $1.4f_1$ . Note that the worst-case oscillator tuning range corresponds to the coverage from  $8f_1$  to approximately  $9f_1$ , reaching 12.5%. The abundance of components between  $f_1$  and  $10f_1$  makes it possible to produce the lower decades by means of power-of-2 dividers.

The topology of Fig. 9 places the burden on the design of the oscillator and the first rank of the dividers (enclosed in the dashed box). For  $f_1 = 10$  GHz, these building blocks must operate at 80 GHz. Fortunately, recent work on millimeter-wave CMOS circuits has demonstrated these capabilities [12, 13, 14]. For example, oscillators and  $\div 2$  circuits operating up to 128 GHz have been reported in 90-nm CMOS technology [14]. However, due to the sublinear increase of inductor  $Q$ 's with frequency and the fall of varactor  $Q$ 's, the oscillator incurs a heavy phase noise-power consumption trade-off.

Another important issue in the topology of Fig. 9 stems from the supply coupling within divider chains. Suppose, for example, the chain producing  $1.45f_1$  is enabled. If the dividers in this chain share the same supply line, then a fraction of the component at  $2.9f_1$  appears in the  $1.45f_1$  output, downconverting interferers at  $2.9f_1$  to the baseband. Thus, symmetry in the layout of these dividers proves critical.

Figure 10(a) depicts an alternative approach to multi-decade carrier synthesis [15]. The circuit consists of a quadrature  $LC$  oscillator operating at one of two frequencies (e.g., 17.5 GHz and 14 GHz) and three divider chains providing divide ratios of 2, 3, 4, 5, 6, 8, and 10. Shown in Fig. 10(b) are the output frequencies, indicating a worst-case oscillator tuning range of 14%.

The circuit produces quadrature phases at all outputs, even those emerging from odd-ratio dividers. An exception to the third principle prescribed above, this is afforded through the use of quadrature Miller dividers [16]. Figure 11(a) shows a  $\div 5$  example, where an SSB mixer and a  $\div 4$  chain form a Miller loop, reaching stable operation if  $(f_{LO} - f_{out})/4 = f_{out}$  [16].

The use of SSB mixing in the  $\div 5$  circuit raises concern with

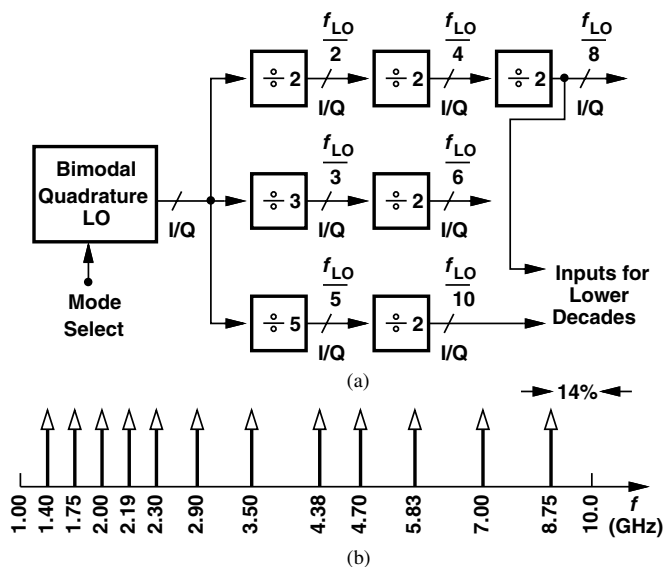


Fig. 10. (a) Multidecade carrier generation using a single bimodal LO, (b) example of frequencies generated.

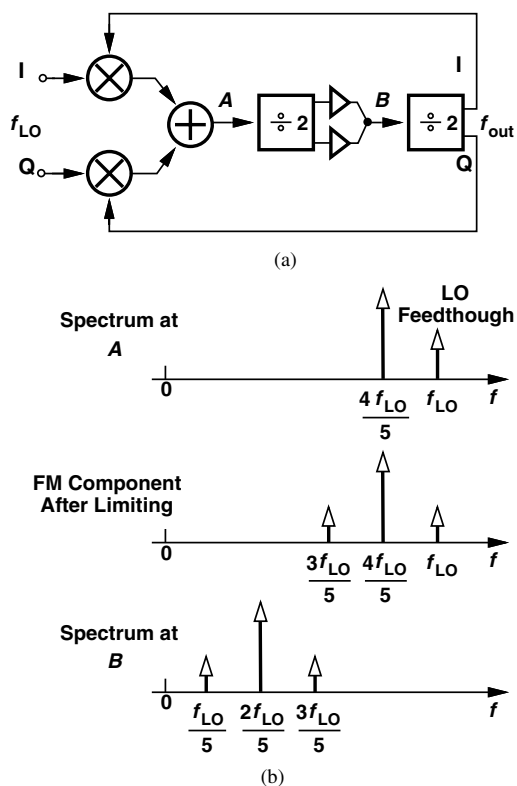


Fig. 11. (a) Divide-by-5 realization [16], (b) problem of spurs at intermediate nodes.

respect to the spurious components. Fortunately, it can be shown that all of the unwanted frequencies generated by the SSB mixer are translated to zero,  $f_{LO}/5$ , or its harmonics as they travel to the output.

One may consider utilizing the frequencies available at the intermediate nodes of the  $\div 5$  circuit—as the topology in [16] does to obtain a ratio of 2.5. However, these nodes do suffer

from spurs. For example, as illustrated in Fig. 11(b), the mixer LO feedthrough can be decomposed into FM and AM components, the latter of which is removed by the limiting action of the first  $\div 2$  stage, thereby yielding another spur at  $3f_{LO}/5$  [15]. Upon division by 2, the two spurs appear symmetrically disposed around  $2f_{LO}/5$ .

The principal drawback of quadrature Miller dividers is the need for quadrature LO inputs. Quadrature oscillators suffer from substantially higher phase noise (in the  $1/f$  regime) than their non-quadrature counterparts [5] and also exhibit two possible—but poorly-controlled—oscillation frequencies [17].

## V. SPECTRUM SENSING

Cognitive radios must sense the spectrum to determine if a channel is available for communication, an operation presenting great challenges to both the receiver and the digital baseband processor. In fact, due to the so-called “shadowing effect,” CRs must detect signal levels well *below* the sensitivities stipulated by standards. Suppose, as shown in Fig. 12, two “primary users,” *A* and *B*, are communicating in a given

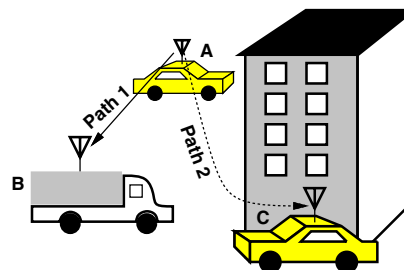


Fig. 12. Shadowing effect in spectrum sensing.

RF channel while a “secondary user,” *C*, wishes to detect the availability of that channel. If located in the “shadow” of an obstacle, user *C* senses only a small power through path 2 even though user *B* receives power at or above the sensitivity level through path 1. In other words, user *C* may decide that the channel is available while it is not. For this reason, CRs must detect signal-to-noise ratios (SNRs) as low as  $-20$  to  $-30$  dB.

While considerable effort has been expended on spectrum sensing algorithms and implementations [18], this task consumes a long time, making it desirable to seek the assistance of the RF and analog sections of the system. This section elaborates on these points.

### A. Sensing Techniques

Among various candidates, two spectrum sensing techniques have emerged as practical contenders: “energy detection” and “feature detection” [18]. The former simply measures the energy in the channel of interest over a sufficiently long period of time so as to average out the effect of the receiver noise, deciding, with a certain probability, whether the channel is available or not. Note that the ADC quantization noise is also averaged out, allowing a resolution of only a few bits.

Though posing minimal burden on digital baseband processing, this technique requires an accurate estimate of the receiver

noise figure (e.g., with 0.1 dB error) if low SNRs must be detected successfully. The noise figure estimation translates to accurate measurement of the receiver gain, which in turn calls for generating an RF tone with a precisely-defined amplitude. This measurement must also be repeated frequently so as to account for temperature drifts of the noise figure and gain.

Spectrum sensing by feature detection seeks “signatures” produced by modulation schemes. Figure 13 shows as an ex-

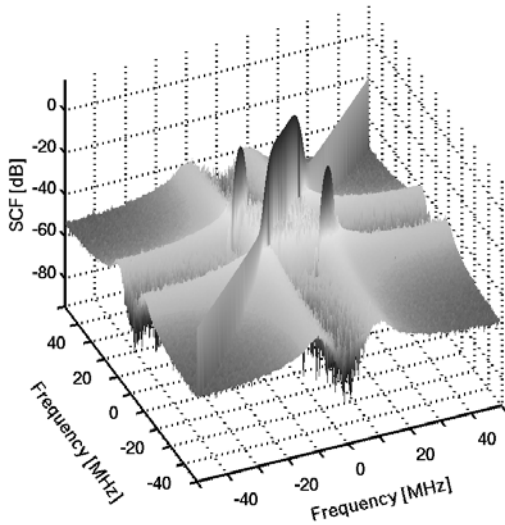


Fig. 13. Spectral correlation function of a QPSK signal.

ample the features corresponding to QPSK modulation. Plotted here is the “spectral correlation function” (SCF), which is obtained by finding the cross correlation between two FFTs of the signal. The two sharp peaks signify a QPSK waveform. Correlating the measured feature with templates of modulation schemes used in each frequency band, the receiver determines whether the channel of interest carries information. In contrast to energy detection, feature detection does not rely on an accurate estimate of the receiver noise figure, relaxing the RF processing but at the cost of more complex digital processing. For example, the ADC resolution must now be higher. Also, the ADC clock frequency offset must remain very small [19].

Perhaps the greatest challenge in spectrum sensing (by energy or feature detection) relates to the *time* necessary to arrive at a reliable decision. As an example, Fig. 14 plots the sensing time required for energy detection of a 4-MHz channel as a function of the SNR [19]. We observe that for an SNR of, say,  $-15$  dB, the sensing consumes about 30 ms, making it difficult for a secondary user to identify an available channel and access the network in a reasonable time. For channel bandwidths as narrow as 30 kHz (used in the cellular bands), the sensing time becomes prohibitively long.

### B. RF-Assisted Spectrum Sensing

In this section, we propose a number of transceiver design techniques that cope with the sensing time problem. In order to raise the probability of finding an available channel, *multiple* channels can be examined concurrently. Illustrated in Fig. 15,

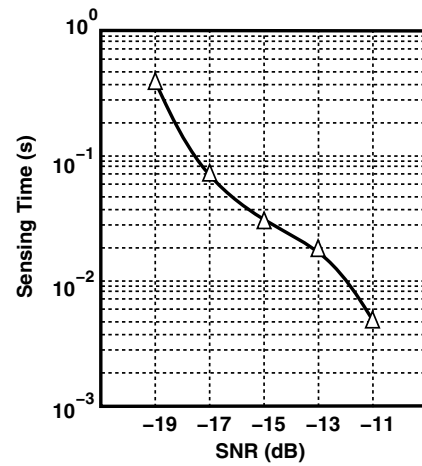


Fig. 14. Spectrum sensing time for a 4-MHz signal [19].

the idea is to downconvert a *block* of channels and digitize

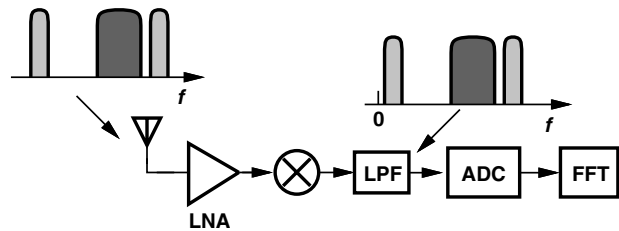


Fig. 15. Block downconversion.

them simultaneously. The baseband processor then takes an FFT of the entire block, revealing the available channels. The sensing performance is now limited by that of the ADC: the wider the block is, the faster the sampling rate and the higher the dynamic range of the ADC must be.

Figure 16(a) illustrates a “two-step” approach. In the first step, the baseband ADC takes a rough snapshot of a block of channels and compares their levels to a threshold, thus identifying “potentially available” channels and dismissing those above the threshold. Note that the LPF bandwidth and the ADC sampling rate must be commensurate with the overall bandwidth of the downconverted block of channels. Also, the ADC dynamic range must accommodate the random summation of all of the large interferers within the block. In the second step, one of the “subthreshold” channels is analyzed for availability.

The above method relaxes the sensing time issue only moderately because the second step still proves to be the bottleneck. Alternatively, the second step can incorporate more complex processing to arrive at an available channel more quickly. As shown in Fig. 16(b), a number of baseband branches can be activated in this step so as to simultaneously “zoom in” onto multiple subthreshold channels. Each bandpass filter (BPF) selects only one such channel, allowing its subsequent ADC to detect the energy or modulation signature therein. For  $n$  additional branches, this architecture examines  $n$  channels in the sensing time of one channel, i.e., it raises the probability of finding an available channel by a factor of  $n$ .

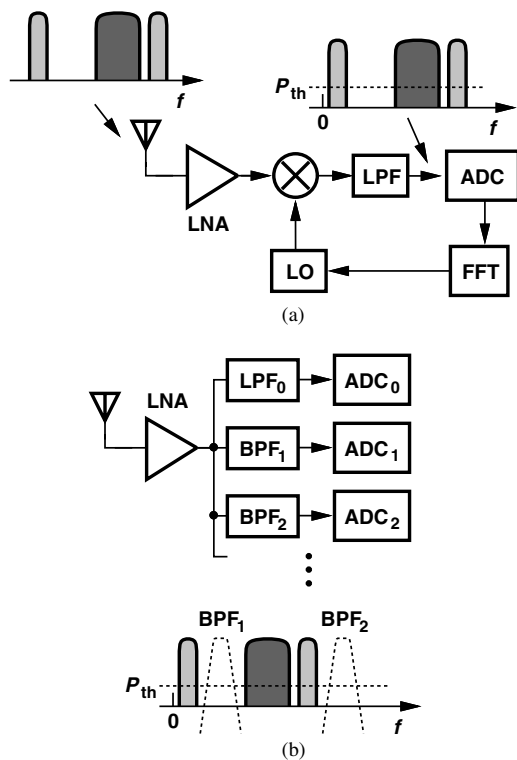


Fig. 16. Two-step spectrum sensing with (a) one channel sensed in the second step, (b) multiple channels sensed in the second step.

The architecture of Fig. 16(b) trades baseband complexity and power dissipation for spectrum sensing time. Fortunately, the BPF/ADC cascades need not be very complex. If the BPF suppresses other channels sufficiently, then the ADC resolution can be as low as a few bits because its quantization noise is averaged out during sensing. With moderate BPF selectivity, the ADC resolution must increase by a few more bits.

#### Acknowledgment

The author wishes to thank Danijela Cabric and Brian Lee for valuable discussions.

#### REFERENCES

[1] J. Mitola and G. Q. Maquire, "Cognitive radio: making software radios more personal," *IEEE Personal Communications*, vol. 6, pp. 13-18, Aug. 1999. Mitola, J., III Maguire, G.Q., Jr.

[2] S. Haykin, "Cognitive radio: brain-empowered wireless communications," *IEEE J. Selected Areas in Communications*, vol. 23, pp. 201-220, Fe. 2005.

[3] J. Park et al, "A Fully-Integrated UHF Receiver with Multi-Resolution Spectrum-Sensing (MRSS) Functionality for IEEE 802.22 Cognitive-Radio Applications," *ISSCC Dig. Tech. papers*, pp. 526-527, Feb. 2008.

[4] S. Shekhar, X. Li, and D. J. Allstot, "A Fully-Integrated UHF Receiver with Multi-Resolution Spectrum-Sensing (MRSS) Functionality for IEEE 802.22 Cognitive-Radio

Applications," *RFIC Symp. Dig. Tech. Papers*, June 2006.

[5] B. Razavi, "Design of Millimeter-Wave CMOS Radios: A Tutorial," *IEEE Trans. Circuits and Systems - Part I*, vol. 56, pp. 4-16, Jan. 2009.

[6] F. Bruccoleri, E. A. M. Klumpernink, and B. Nauta, "Wide-band CMOS low-noise amplifier exploiting thermal noise canceling," *IEEE J. Solid-State Circuits*, vol. 39, pp. 275-282, Feb. 2004.

[7] D. Manstretta, M. Brandolini, and F. Svelto, "Second-order intermodulation mechanisms in CMOS downconverters," *IEEE J. Solid-State Circuits*, vol. 38, pp. 394-406, March 2003.

[8] M. Brandolini et al, "A +78 dBm IIP2 CMOS direct downconversion mixer for fully integrated UMTS receivers," *IEEE J. Solid-State Circuits*, vol. 41, pp. 552-559, March 2006.

[9] Z. Ru et al, "A Software-Defined Radio Receiver Architecture Robust to Out-of-Band Interference," *ISSCC Dig. Tech. papers*, pp. 230-231, Feb. 2009.

[10] N. A. Moseley et al, "A 400-to-900 MHz Receiver with Dual-Domain Harmonic Rejection Exploiting Adaptive Interference Cancellation," *ISSCC Dig. Tech. papers*, pp. 232-233, Feb. 2009.

[11] J. A. Weldon et al, "A 1.75-GHz highly integrated narrow-band CMOS transmitter with harmonic-rejection mixers," *IEEE J. Solid-State Circuits*, vol. 36, pp. 2003-2015, Dec. 2001.

[12] H.-H. Hsieh and L. H. Lu, "A 63-GHz VCO in 0.18- $\mu$ m CMOS Technology," *Symposium on VLSI Circuits Dig. Of Tech. Papers*, pp. 178-179, June 2007.

[13] K.-H. Tsai et al, "3.5mW W-Band Frequency Divider with Wide Locking Range in 90nm CMOS Technology," *ISSCC Dig. Tech. Papers*, pp. 466-467, Feb. 2008.

[14] B. Razavi, "A Millimeter-Wave Circuit Technique," *IEEE J. Solid-State Circuits*, vol. 43, pp. 477-485, Sept. 2008.

[15] B. Razavi, "Multi-Decade Carrier Generation for Cognitive Radios," to be presented at Symp. on VLSI Circuits, Kyoto, June 2009.

[16] C.-C. Lin and C.-K. Wang, "A regenerative semi-dynamic frequency divider for mode-1 MB-OFDM UWB hopping carrier generation," *ISSCC Dig. Tech. Papers*, pp. 206-207, Feb. 2005.

[17] S. Li, I. Kipnis, and M. Ismail, "A 10-GHz CMOS quadrature LC-VCO for multirate optical applications," *IEEE J. Solid-State Circuits*, vol. 38, pp. 1626-1634, Oct. 2003.

[18] D. Cabric, S. M. Mishra, and R. W. Brodersen, "Implementation issues in spectrum sensing for cognitive radios," *Conf. Rec. of 38th Asilomar Conference on Signals, Systems, and Computers*, Nov. 2004.

[19] D. Cabric, *Cognitive Radios: System Design Perspective*, PhD Dissertation, University of California, Berkeley, 2007.